EUROPEAN ORGANIZATION FOR NUCLEAR RESEARCH

CERN-PPE/91-214
4 December 1991

An improved measurement of $\alpha_S(M_{Z^0})$ using energy correlations with the OPAL detector at LEP

The OPAL Collaboration

Abstract

We report on an improved measurement of the value of the strong coupling constant α_S at the Z^0 peak, using the asymmetry of the energy-energy correlation function. The analysis, based on second order perturbation theory and a data sample of about 145,000 multihadronic Z^0 decays, yields

$$\alpha_S(M_{Z^0}) = 0.118 \pm 0.001\,(\text{stat.}) \pm 0.003\,(\text{exp.syst.})\,^{+0.009}_{-0.004}\,(\text{theor.syst.})\,,$$

where the theoretical systematic error accounts for uncertainties due to hadronization, the choice of the renormalization scale and unknown higher order terms. We adjust the parameters of a second order matrix element Monte Carlo followed by string hadronization to best describe the energy correlation and other hadronic Z^0 decay data. The α_S result obtained from this second order Monte Carlo is found to be unreliable if values of the renormalization scale smaller than about $0.15 \cdot E_{c.m.}$ are used in the generator.

(Submitted to Physics Letters B)

The OPAL Collaboration

P.D. Acton[25], G. Alexander[23], J. Allison[16], P.P. Allport[5], K.J. Anderson[9], S. Arcelli[2], P. Ashton[16], A. Astbury[a], D. Axen[b], G. Azuelos[18,c], G.A. Bahan[16], J.T.M. Baines[16], A.H. Ball[17], J. Banks[16], G.J. Barker[13], R.J. Barlow[16], J.R. Batley[5], G. Beaudoin[18], A. Beck[23], J. Becker[10], T. Behnke[27], K.W. Bell[20], G. Bella[23], P. Berlich[10], S. Bethke[11], O. Biebel[3], U. Binder[10], I.J. Bloodworth[1], P. Bock[11], B. Boden[3], H.M. Bosch[11], S. Bougerolle[b], B.B. Brabson[12], H. Breuker[8], R.M. Brown[20], R. Brun[8], A. Buijs[8], H.J. Burckhart[8], P. Capiluppi[2], R.K. Carnegie[6], A.A. Carter[13], J.R. Carter[5], C.Y. Chang[17], D.G. Charlton[8], P.E.L. Clarke[25], I. Cohen[23], W.J. Collins[5], J.E. Conboy[15], M. Cooper[22], M. Couch[1], M. Coupland[14], M. Cuffiani[2], S. Dado[22], G.M. Dallavalle[2], S. De Jong[8], P. Debu[21], L.A. del Pozo[5], M.M. Deninno[2], A. Dieckmann[11], M. Dittmar[4], M.S. Dixit[7], E. Duchovni[26], G. Duckeck[11], I.P. Duerdoth[16], D.J.P. Dumas[6], G. Eckerlin[11], P.A. Elcombe[5], P.G. Estabrooks[6], E. Etzion[23], F. Fabbri[2], M. Fincke-Keeler[a], H.M. Fischer[3], D.G. Fong[17], C. Fukunaga[24], A. Gaidot[21], O. Ganel[26], J.W. Gary[4], J. Gascon[18], R.F. McGowan[16], N.I. Geddes[20], C. Geich-Gimbel[3], S.W. Gensler[9], F.X. Gentit[21], G. Giacomelli[2], V. Gibson[5], W.R. Gibson[13], J.D. Gillies[20], J. Goldberg[22], M.J. Goodrick[5], W. Gorn[4], C. Grandi[2], F.C. Grant[5], J. Hagemann[27], G.G. Hanson[12], M. Hansroul[8], C.K. Hargrove[7], P.F. Harrison[13], J. Hart[5], P.M. Hattersley[1], M. Hauschild[8], C.M. Hawkes[8], E. Heflin[4], R.J. Hemingway[6], R.D. Heuer[8], J.C. Hill[5], S.J. Hillier[1], D.A. Hinshaw[18], C. Ho[4], J.D. Hobbs[8], P.R. Hobson[25], D. Hochman[26], B. Holl[8], R.J. Homer[1], A.K. Honma[e], S.R. Hou[17], C.P. Howarth[15], R.E. Hughes-Jones[16], R. Humbert[10], P. Igo-Kemenes[11], H. Ihssen[11], D.C. Imrie[25], A.C. Janissen[6], A. Jawahery[17], P.W. Jeffreys[20], H. Jeremie[18], M. Jimack[2], M. Jobes[1], R.W.L. Jones[13], P. Jovanovic[1], D. Karlen[6], K. Kawagoe[24], T. Kawamoto[24], R.K. Keeler[a], R.G. Kellogg[17], B.W. Kennedy[15], C. Kleinwort[8], D.E. Klem[19], T. Kobayashi[24], T.P. Kokott[3], S. Komamiya[24], L. Köpke[8], J.F. Kral[8], R. Kowalewski[6], H. Kreutzmann[3], J. von Krogh[11], J. Kroll[9], M. Kuwano[24], P. Kyberd[13], G.D. Lafferty[16], F. Lamarche[18], W.J. Larson[4], J.G. Layter[4], P. Le Du[21], P. Leblanc[18], A.M. Lee[17], M.H. Lehto[15], D. Lellouch[26], P. Lennert[11], C. Leroy[18], J. Letts[4], S. Levegrün[3], L. Levinson[26], S.L. Lloyd[13], F.K. Loebinger[16], J.M. Lorah[17], B. Lorazo[18], M.J. Losty[7], X.C. Lou[12], J. Ludwig[10], M. Mannelli[8], S. Marcellini[2], G. Maringer[3], A.J. Martin[13], J.P. Martin[18], T. Mashimo[24], P. Mättig[3], U. Maur[3], J. McKenna[a], T.J. McMahon[1], J.R. McNutt[25], F. Meijers[8], D. Menszner[11], F.S. Merritt[9], H. Mes[7], A. Michelini[8], R.P. Middleton[20], G. Mikenberg[26], J. Mildenberger[6], D.J. Miller[15], R. Mir[12], W. Mohr[10], C. Moisan[18], A. Montanari[2], T. Mori[24], M.W. Moss[16], T. Mouthuy[12], B. Nellen[3], H.H. Nguyen[9], M. Nozaki[24], S.W. O'Neale[8,d], B.P. O'Neill[4], F.G. Oakham[7], F. Odorici[2], M. Ogg[6], H.O. Ogren[12], H. Oh[4], C.J. Oram[e], M.J. Oreglia[9], S. Orito[24], J.P. Pansart[21], B. Panzer-Steindel[8], P. Paschievici[26], G.N. Patrick[20], S.J. Pawley[16], P. Pfister[10], J.E. Pilcher[9], J.L. Pinfold[26], D. Pitman[a], D.E. Plane[8], P. Poffenberger[a], B. Poli[2], A. Pouladdej[6], E. Prebys[8], T.W. Pritchard[13], H. Przysiezniak[18], G. Quast[27], M.W. Redmond[9], D.L. Rees[1], K. Riles[4], S.A. Robins[13], D. Robinson[8], A. Rollnik[3], J.M. Roney[9], E. Ros[8], S. Rossberg[10], A.M. Rossi[2,f], M. Rosvick[a], P. Routenburg[6], K. Runge[10], O. Runolfsson[8], D.R. Rust[12], S. Sanghera[6], M. Sasaki[24], A.D. Schaile[10], O. Schaile[10], W. Schappert[6], P. Scharff-Hansen[8], P. Schenk[a], H. von der Schmitt[11], S. Schreiber[3], J. Schwiening[3], W.G. Scott[20], M. Settles[12], B.C. Shen[4], P. Sherwood[15], R. Shypit[b], A. Simon[3], P. Singh[13], G.P. Siroli[2], A. Skuja[17], A.M. Smith[8], T.J. Smith[8], G.A. Snow[17], R. Sobie[g], R.W. Springer[17], M. Sproston[20], K. Stephens[16], H.E. Stier[10,†], R. Ströhmer[11], D. Strom[9], H. Takeda[24], T. Takeshita[24], P. Taras[18], S. Tarem[26], P. Teixeira-Dias[11], N.J. Thackray[1],

G. Transtromer[25], T. Tsukamoto[24], M.F. Turner[5], G. Tysarczyk-Niemeyer[11], D. Van den plas[18], R. Van Kooten[8], G.J. VanDalen[4], G. Vasseur[21], C.J. Virtue[19], A. Wagner[27], C. Wahl[10], J.P. Walker[1], C.P. Ward[5], D.R. Ward[5], P.M. Watkins[1], A.T. Watson[1], N.K. Watson[8], M. Weber[11], P. Weber[6], S. Weisz[8], P.S. Wells[8], N. Wermes[11], M. Weymann[8], M.A. Whalley[1], G.W. Wilson[21], J.A. Wilson[1], I. Wingerter[8], V-H. Winterer[10], N.C. Wood[16], S. Wotton[8], T.R. Wyatt[16], R. Yaari[26], Y. Yang[4,h], G. Yekutieli[26], M. Yurko[18], I. Zacharov[8], W. Zeuner[8], G.T. Zorn[17].

[1]School of Physics and Space Research, University of Birmingham, Birmingham, B15 2TT, UK
[2]Dipartimento di Fisica dell' Università di Bologna and INFN, Bologna, 40126, Italy
[3]Physikalisches Institut, Universität Bonn, D-5300 Bonn 1, FRG
[4]Department of Physics, University of California, Riverside, CA 92521 USA
[5]Cavendish Laboratory, Cambridge, CB3 0HE, UK
[6]Carleton University, Dept of Physics, Colonel By Drive, Ottawa, Ontario K1S 5B6, Canada
[7]Centre for Research in Particle Physics, Carleton University, Ottawa, Ontario K1S 5B6, Canada
[8]CERN, European Organisation for Particle Physics, 1211 Geneva 23, Switzerland
[9]Enrico Fermi Institute and Department of Physics, University of Chicago, Chicago Illinois 60637, USA
[10]Fakultät für Physik, Albert Ludwigs Universität, D-7800 Freiburg, FRG
[11]Physikalisches Institut, Universität Heidelberg, Heidelberg, FRG
[12]Indiana University, Dept of Physics, Swain Hall West 117, Bloomington, Indiana 47405, USA
[13]Queen Mary and Westfield College, University of London, London, E1 4NS, UK
[14]Birkbeck College, London, WC1E 7HV, UK
[15]University College London, London, WC1E 6BT, UK
[16]Department of Physics, Schuster Laboratory, The University, Manchester, M13 9PL, UK
[17]Department of Physics and Astronomy, University of Maryland, College Park, Maryland 20742, USA
[18]Laboratoire de Physique Nucléaire, Université de Montréal, Montréal, Quebec, H3C 3J7, Canada
[19]National Research Council of Canada, Herzberg Institute of Astrophysics, Ottawa, Ontario K1A 0R6, Canada
[20]Rutherford Appleton Laboratory, Chilton, Didcot, Oxfordshire, OX11 0QX, UK
[21]DPhPE, CEN Saclay, F-91191 Gif-sur-Yvette, France
[22]Department of Physics, Technion-Israel Institute of Technology, Haifa 32000, Israel
[23]Department of Physics and Astronomy, Tel Aviv University, Tel Aviv 69978, Israel
[24]International Centre for Elementary Particle Physics and Dept of Physics, University of Tokyo, Tokyo 113, and Kobe University, Kobe 657, Japan
[25]Brunel University, Uxbridge, Middlesex, UB8 3PH UK
[26]Nuclear Physics Department, Weizmann Institute of Science, Rehovot, 76100, Israel
[27]Universität Hamburg/DESY, II Inst. für Experimental Physik, 2000 Hamburg 52, FRG

[a]University of Victoria, Dept of Physics, P O Box 3055, Victoria BC V8W 3P6, Canada
[b]University of British Columbia, Dept of Physics, 6224 Agriculture Road, Vancouver BC V6T 1Z1, Canada
[c]Also at TRIUMF, Vancouver, Canada V6T 2A3

[d]On leave from Birmingham University, Birmingham B15 2TT, UK
[e]Univ of Victoria, Dept of Physics, P.O. Box 1700, Victoria BC V8W 2Y2, Canada and TRIUMF, Vancouver, Canada V6T 2A3
[f]Present address: Dipartimento di Fisica, Università della Calabria and INFN, 87036 Rende, Italy
[g]University of British Columbia, Dept of Physics, 6224 Agriculture Road, Vancouver BC V6T 2A6, Canada and IPP, McGill University, High Energy Physics Department, 3600 University Str, Montreal, Quebec H3A 2T8, Canada
[h]On leave from Research Institute for Computer Peripherals, Hangzhou, China
[†]deceased 25th March 1991

1 Introduction

The energy-energy correlation function $\Sigma_{EEC}(\chi)$ [1] has been one of the most widely used variables for the measurement of the strong coupling constant α_S in e^+e^- annihilations [2]-[6]. It is defined in terms of the angle χ_{ij} between two particles i and j in a multihadronic event:

$$\Sigma_{EEC}(\chi) = \frac{1}{\Delta\chi \cdot N_{events}} \sum_{N_{events}} \int_{\chi-\Delta\chi/2}^{\chi+\Delta\chi/2} \sum_{i,j} \frac{E_i E_j}{E_{vis.}^2} \cdot \delta(\chi' - \chi_{ij})\, d\chi' \; ; \tag{1}$$

E_i and E_j are the energies of particles i and j; $E_{vis.}$ is the sum over the energies of all observed particles in the event; $\Delta\chi$ is the angular bin width. The distribution is summed over all events in the sample under study, as indicated. The normalization is such that the integral of $\Sigma_{EEC}(\chi)$ from $\chi = 0°$ to $\chi = 180°$ is unity.

Two-jet events contribute to Σ_{EEC} at values of χ near 0° and 180°. The contributions for $\chi \approx 0°$ arise from correlations between particles in the same jet while the contributions for $\chi \approx 180°$ arise from correlations between particles in the opposing jets. For events with three or more jets, the Σ_{EEC} distribution is populated at $\chi \approx 0°$ and at central values of χ. The height of Σ_{EEC} for the central values is thus a measure of the rate of hard, acolinear gluon radiation and of α_S.

Because of the energy weighting, the region around $\chi = 0°$ is primarily populated by the highest energy jet in an event: relative to these jets the radiated gluon jets usually appear in the opposite hemisphere, corresponding to $\chi > 90°$. This suggests the introduction of the asymmetry distribution $\Sigma_{AEEC}(\chi)$ [1] around the value $\chi = 90°$, defined by

$$\Sigma_{AEEC}(\chi) = \Sigma_{EEC}(180° - \chi) - \Sigma_{EEC}(\chi) \; . \tag{2}$$

The subtraction in (2) leads to cancellation of the two-jet component and of theoretical and experimental errors which contribute symmetrically to Σ_{EEC}. Therefore Σ_{AEEC} has smaller systematic uncertainties than Σ_{EEC}. Note that the two-jet component is not useful for a determination of α_S to second order. In contrast to other measures of α_S such as jet rates, energy correlations are entirely inclusive and do not require a definition of jets. They are thereby free of theoretical ambiguities related to the so-called jet recombination scheme [7]. Furthermore, the Σ_{AEEC} distribution at second order has been shown to be essentially independent of the choice of the renormalization scale [3]-[6]. In contrast, the α_S results from many other distributions show a strong dependence on this scale. This leads to the expectation that Σ_{AEEC} should provide one of the most accurate measurements of α_S from e^+e^- annihilations at the Z^0 energy, before extensions to the second order theory become available for jet rates and other quantities.

In this letter, we report on a measurement of α_S using the energy correlation asymmetry at the Z^0 peak, performed with the multihadronic data sample of OPAL. This is an update of our previous study of energy correlations [3]. Improved understanding of detector performance and increased data statistics lead to a reduction on the error of $\alpha_S(M_{Z^0})$ relative to what was obtained in this earlier publication.

2 Data sample

A detailed description of the OPAL detector is given in [8]. The detector elements most relevant for this analysis are a large volume central tracking detector and an electromagnetic calorimeter composed of lead glass blocks. The tracking chamber provides up to 159 measured space points and close to 100% tracking efficiency for the detection of charged tracks in the polar angle region $|\cos\theta| < 0.92$: the average angular resolution which is currently achieved is about 0.1 mrad in the plane perpendicular to the beam axis and better than 10 mrad in the direction which includes it. Energy deposits in the electromagnetic calorimeter ("clusters") are measured for over 98% of the solid angle with the calorimeter. Each lead glass block subtends approximately 40 mrad x 40 mrad.

The trigger and multihadronic event selection are discussed in [9] and [10]. For this analysis, additional criteria were applied in order to eliminate poorly measured tracks and to obtain well contained events. Charged tracks were accepted if they originated from within 5 cm of the interaction point in the direction perpendicular to the beam pipe and from within 25 cm in the direction along it. Each charged track was required to have a transverse momentum with respect to the beam direction of more than 150 MeV/c and at least 40 measured space points. Clusters were accepted if they had over 200 MeV of energy and were spread over at least two lead glass blocks. Hadronic events were required to contain at least five charged tracks which satisfied the above criteria and a polar angle θ_{thrust} for the thrust axis, defined using the accepted charged tracks and clusters, which satisfied $|\cos\theta_{thrust}| < 0.9$. In about 1% of the events, a charged track was reconstructed with a momentum value larger than the beam energy: if this momentum value was larger than 60 GeV/c, the event was rejected. Starting from a data sample of about 6.5 pb^{-1}, corresponding to approximately 145,000 multihadronic events collected by OPAL in 1990, we obtained 128,032 events after application of these cuts. The average center-of-mass energy, $E_{c.m.}$, was 91.3 GeV. Only charged tracks and clusters which satisfied the above criteria were used for the subsequent analysis.

For systematic studies which are discussed below, we also selected data samples using either charged tracks only or calorimeter clusters only. For the sample based on charged tracks only, the same track and event selections as given above were used, leading to 134,148 events. For the sample based on calorimeter clusters only, the same cluster and event selections as given above were used except that eight accepted clusters were required to be present in an event instead of five charged tracks: this yielded 126,674 events.

3 Energy correlation measurements

The measured energy correlation distribution and its asymmetry are shown in figure 1; the numerical values are given in table 1. The distributions have been unfolded for detector acceptance and resolution and for initial-state photon radiation using a bin-by-bin correction procedure which is described in [3]. For the measurements, both charged tracks and clusters are used. The bin widths of 1° are well within the limits of the experimental angular resolution. The unfolded Σ_{AEEC} is derived from the unfolded Σ_{EEC}: this yields smaller statistical fluctuations than the case when the unfolded asymmetry distribution is obtained by correcting the

measured one directly. The bin-by-bin correction constants are derived from the Jetset parton shower model [11], version 7.2, with Lund string hadronization, in conjunction with a detailed simulation of the OPAL detector [12]. The parameter values of Jetset have been adjusted by OPAL to describe global event shape measurements [13]. This model, used in conjunction with simulation of the detector, provides an excellent description of the energy correlation measurements before the corrections are applied, making it appropriate for the calculation of the correction constants. Except for the first few bins, for which the corrections are about 20%, the values of the corrections lie between 0.93 and 1.09.

The statistical errors of the Σ_{EEC} and Σ_{AEEC} distributions have strong bin-to-bin correlations because of the jet structure of the events. To evaluate these errors, we therefore generated 10 different samples of Monte Carlo events, each with the same statistics as the data sample. The statistical error was set equal to the rms deviation which was observed, for each bin. Two sources of systematic uncertainty were considered: (1) the error due to imperfections in the simulation program and in event reconstruction and (2) the model dependence of the correction factors. The error due to imperfections in the simulation of the detector and event reconstruction was estimated by calculating the unfolded Σ_{AEEC} distribution using only charged track measurements and comparing this to the corresponding result obtained using only cluster measurements: the error was defined to be the full difference between these two. The error due to the model dependence of the correction procedure was determined by using a mock data sample generated with the Herwig shower model [14], version 5.0, with detector simulation, and then applying the same Jetset derived correction constants that are applied to the data. Herwig, in contrast to Jetset, uses a cluster mechanism to describe hadronization. The Herwig parameter values have also been adjusted by OPAL to describe the global characteristics of multihadronic Z^0 decays, using the technique presented in [13].[1] The difference between the unfolded Herwig "data" distribution and the Herwig distribution constructed at the generator level with the same parameter set was taken to be the systematic error introduced by the correction procedure, bin-by-bin. The two sources of systematic errors were added in quadrature to define the total systematic error.

Shown in figure 1 (a) and (b), in comparison to the data, are the hadron level predictions of Herwig and the Cojets [15] parton shower model, version 6.12. Cojets employs an independent model for quark and gluon hadronization and so provides a third alternative to describe this process, which differs from the string mechanism of Jetset and the cluster one of Herwig. The parameter values of Cojets have been tuned by its author [16] to describe global event shape measurements of OPAL. Quark and gluon jets have identical properties for this version of Cojets and the model does not describe OPAL measurements of the string effect [17] or quark-gluon jet differences [18]. It is seen that Cojets also does not describe the Σ_{AEEC} distribution well, for χ values smaller than about 40°. Herwig also shows an important discrepancy with the energy asymmetry data, for values of χ larger than about 40°. Jetset, in contrast, agrees very well with our measurements: we do not include the Jetset curve in figure 1 (a) and (b) as it would obscure the presentation of our data. The excellent agreement of Jetset with the energy correlation measurements is visible in figure 1 (c) and (d), which shows the deviation

[1] For Herwig version 5.0, we find QCDLAM=0.20, VGCUT=0.06, VQCUT=0.48 and CLMAX=3.5 for the main parameters which control the momentum distribution of particles: these parameter values, which are now the default ones of Herwig, lead to essentially the same description of global event shape distributions and the mean charged multiplicity in Z^0 decays as do the parameter set presented for Herwig version 3.4 in [13].

of the model predictions from the data in units of standard deviation, for Σ_{EEC} and Σ_{AEEC}, respectively. The standard deviation is defined using the full statistical and systematic errors of the data points. The Jetset curve is essentially always within one standard deviation of the data points; Herwig and Cojets show much larger deviations from the data.

4 Measurement of $\alpha_S(M_{Z^0})$

To determine α_S, the measured Σ_{EEC} distribution is corrected for the effects of hadronization: the corrected Σ_{AEEC} distribution is derived from the corrected Σ_{EEC}, as before. The integral of Σ_{AEEC} between 30° and 90° is then calculated and compared to the predictions of second order perturbation theory. We employ two different strategies to correct for hadronization; one makes use of a parton shower and the other of a second order matrix element Monte Carlo:

(1) The data are corrected to the level of quarks and gluons using the Jetset parton shower model, with a cutoff on the perturbative evolution of $Q_0 = 1$ GeV/c^2, where Q_0 is the effective virtual mass of the partons. The data so corrected are compared to the second order analytic formula of Kunszt and Nason [7], valid for massless partons corresponding to $Q_0 \approx 0$ GeV/c^2. A renormalization scale $\mu = M_{Z^0}$ is used for the argument of $\alpha_S(\mu)$ in the theoretical formula. The 1 GeV/c^2 difference between the parton virtuality of the theory and corrected data is small compared to the scale of the jet energies and is not expected to be important: thus experiment and theory use a consistent definition of the parton state in this comparison.[2] Since the corrections do not include the effects of unknown higher order terms, the goodness of description of the data by the theory – and the consistency found between this measurement and other measurements of α_S – is a test of the adequacy of the second order calculations, as is discussed in [7]. The Jetset parton shower model provides a very good description of the global characteristics of hadronic events in e^+e^- annihilations over a wide range of center-of-mass energies, using an energy independent parameterization of the hadronization [13]. This implies that the hadronization corrections obtained from this model are reliable. To obtain the corrected data in this strategy using a parton shower, the unfolding is applied from the level including detector effects to the parton level, in one step, without use of the hadron level corrected measurements of figure 1.

(2) The data are corrected to the parton level using a second order matrix element Monte Carlo. The ERT second order equations [19] – available as a non-default option in Jetset – are used, with Lund string hadronization for the quarks and gluons. The model parameters are tuned to describe hadron level measurements before the corrections are calculated. The value of the renormalization scale is again chosen to be $\mu = M_{Z^0}$ to correspond to the choice above (see also the discussion in section 4.4). Resolvable parton jets[3] are defined using the y_{min}

[2] The mean number of partons $< n_p >$ which are present at the end of the perturbative shower has been sometimes used in the literature to measure the consistency between the parton shower and second order calculations: however $< n_p >$ depends on details of the Monte Carlo algorithms, i.e. $< n_p >$ is about 9.2 in Jetset and 6.7 in Herwig in hadronic Z^0 decays, for similar values of the parton shower cutoff.

[3] The need to introduce parton jet resolution criteria for the analysis based on the second order Monte Carlo is an artifact of the Monte Carlo method, because it is necessary to have a positive value of the *total* cross section for 2-, 3- and 4-jet production, individually, and is not related to any property of the energy correlation distributions themselves.

value $y_{min} = 0.01$, which is the minimum scaled pair mass m_{ij} allowed for two partons i and j through the relation $(m_{ij}/E_{c.m.})^2 > y_{min}$. The value of $y_{min} = 0.01$ is favored by experimental studies at PEP and PETRA and is the recommended value for studies at LEP [20]. The corrected measurements are compared to the theoretical expectation derived from the same second order Monte Carlo, without hadronization. Thus, again, the definition of the parton state is consistent between the theory and the corrected data: in this case it corresponds to a level of parton virtuality of $Q_0 \approx 9$ GeV/c^2, because of the non-zero value chosen for y_{min}. In this second strategy to estimate the hadronization corrections, the corrections are assumed to include a large part of the unknown higher order terms, which are approximated by the phenomenological hadronization model in this case. In this sense, this strategy presents an extreme choice relative to the first, parton shower based strategy. For this second strategy, the data are corrected to the parton level starting with the hadron level corrected measurements shown in figure 1. This two step correction procedure has the advantage that the detector and hadronization corrections are separated. We thereby avoid a possible bias pointed out in [21], which can be introduced when a second order Monte Carlo is used both to unfold for detector effects and to determine α_S.

We next present the details of these two different analyses. Our final result for α_S will be based on the strategy which uses the parton shower corrections because of the excellent description of the data that is obtained with this model. For this same reason, the parton shower strategy will be used to evaluate most of the systematic uncertainties, including the experimental one. The result which is based on corrections from the second order Monte Carlo will be used to determine the systematic error on α_S due to the unknown higher order perturbative terms.

4.1 Method using analytic formula

Figure 2 summarizes our results from the parton shower method to correct for hadronization. The horizontal bands show the values of the corrected $\Sigma_{AEEC}(\chi)$ distribution, integrated between 30° and 90°, which are obtained under various conditions. Three bands are obtained using Jetset for the corrections: one uses charged tracks only for the experimental measurements, one uses clusters only and one uses both. Also shown are the results obtained using hadronization corrections from Herwig and Cojets. The widths of the bands represent the statistical errors.

The solid curve in figure 2 shows the prediction of the Kunszt and Nason second order formula. The theoretical results are shown as a function of the scale parameter $\Lambda_{\overline{MS}}$ of strong interactions. We relate $\Lambda_{\overline{MS}}$ to $\alpha_S(M_{Z^0})$ using the second order expression given in [22]. The intersection of the theoretical curve with the data values defines the measurement of $\Lambda_{\overline{MS}}$. Also shown in figure 2 are theoretical curves derived from the second order calculations of Falck and Kramer [23] and of Richards, Stirling and Ellis [24]. These last two calculations will be discussed in section 4.3. The results presented in this section are based on the Kunszt-Nason formula.

From figure 2 we extract the following:

1. $\Lambda_{\overline{MS}} = 220 \pm 9$ MeV (stat.), using the Jetset corrected data value based on both charged tracks and clusters;

2. a systematic error on $\Lambda_{\overline{MS}}$, due to imperfections in the detector simulation or event reconstruction, of 25 MeV, defined to be the maximum of the difference between the three $\Lambda_{\overline{MS}}$ values obtained with Jetset corrections: based on charged track measurements only, cluster measurements only or on both.

We perform a similar analysis to the one shown in figure 2 to evaluate the following additional systematic uncertainties on $\Lambda_{\overline{MS}}$:

3. an error of 22 MeV, obtained by changing the hadronization parameters of Jetset before correcting the data, using the one standard deviation limits given in [13], and taking the maximum of the difference between the resulting values of $\Lambda_{\overline{MS}}$ and the value of 220 MeV quoted above[4];

4. an error of 20 MeV obtained by using lower limits of $\chi = 22°$ and $\chi = 38°$ for the integral of Σ_{AEEC}, instead of the value of $\chi = 30°$ used for figure 2, and taking the maximum of the difference which is found for $\Lambda_{\overline{MS}}$ relative to 220 MeV.

The systematic uncertainty labeled 3 in the above list is our definition of the error associated with the hadronization correction. We do not use Herwig or Cojets to evaluate this uncertainty because these two models describe the energy asymmetry data poorly, as discussed above. It is seen from figure 2 that Herwig and Cojets yield $\Lambda_{\overline{MS}}$ values of 170 ± 8 and 93 ± 7 MeV, respectively (statistical errors only), should they nonetheless be used for this correction. We view these Herwig and Cojets derived results as unrealistic. If the lower limit used for the integral of Σ_{AEEC} is increased from 30° to 45°, to correspond to the region of the measured energy correlation asymmetry distribution which is best described by Cojets (figure 1 (b) and (d)), the $\Lambda_{\overline{MS}}$ result from Herwig increases to about 230 MeV, while the results from Jetset and Cojets remain the same as quoted above, to within the errors.

4.2 Method using matrix element Monte Carlo

The results from the analysis which uses the second order matrix element Monte Carlo for the hadronization corrections are summarized in figure 3. This figure is constructed like figure 2: the data points labeled (1), (2) and (3) show the measured value of the Σ_{AEEC} distribution after it is corrected to the parton level and integrated from 30° to 90°. In this case the data are not displayed as horizontal bands but for specific values of $\Lambda_{\overline{MS}}$, corresponding to different choices of $\Lambda_{\overline{MS}}$ used to calculate the Monte Carlo corrections, as discussed below. The theoretical prediction – derived from the second order Monte Carlo – is shown by the solid line, as a function of $\Lambda_{\overline{MS}}$. Also shown is the result from an analytic calculation of Falck and Kramer, valid, like the Monte Carlo, for $y_{min} = 0.01$. The Falck-Kramer result will be discussed in section 4.3.

[4]The data are corrected for hadronization starting from the hadron level data of figure 1; we change the parameters PARJ(21) and PARJ(41) by $\pm 1\sigma$ as given in table 1 of [13] before calculating the hadronization corrections.

Before calculating the hadronization correction, the parameters of the second order Monte Carlo were optimized to describe hadron level data. The optimization procedure was similar to that presented in [13]. The overall χ^2 value between the model and data for the eight global event shape distributions discussed in [13] was minimized. In addition, the mean charged multiplicity $< n_{ch.} >$ was constrained to lie in the interval between 21.0 and 21.8.[5] The parameter values which we obtained are given in the third column of table 2: in particular we find $\Lambda_{\overline{MS}} = 280$ MeV. We denote this parameter set as ERT-MC-1. The resulting χ^2 values between the ERT-MC-1 model and the event shape data from [13] are listed in the third column of table 3, along with the model result for $< n_{ch.} >$.

The data point labeled (1) in figure 3 shows the measured, integrated value of the Σ_{AEEC} distribution which is obtained after applying hadronization corrections from the ERT-MC-1 model. Through comparison with the theoretical curve, a value $\Lambda_{\overline{MS}} \approx 330$ MeV is extracted from this analysis (cf. the dashed lines in figure 3). We therefore retune the second order Monte Carlo, using the same procedure as before, but this time with $\Lambda_{\overline{MS}}$ fixed at 330 MeV. The result from this second iteration of model tuning is shown by the point labeled (2) in figure 3: we now obtain $\Lambda_{\overline{MS}} = 350$ MeV (cf. the dotted lines in figure 3). Repeating the tuning procedure a third time, with $\Lambda_{\overline{MS}}$ fixed at 350 MeV, yields the point labeled (3) in figure 3: again we obtain $\Lambda_{\overline{MS}} = 350$ MeV. We take this to be the final result from this second order Monte Carlo method to derive the hadronization corrections. This leads to

5. an error on $\Lambda_{\overline{MS}}$ of +130 MeV, defined by the difference between the result found using hadronization corrections and theoretical predictions from the second order Monte Carlo, relative to the result found using the parton shower Monte Carlo and analytic calculations; this is taken to be the uncertainty due to the unknown higher order perturbative terms.

The parameter values from this final iteration of model tuning – denoted ERT-MC-2 – are given in the fourth column of table 2: the resulting χ^2 values with the event shape data and the result for $< n_{ch.} >$ are listed in the fourth column of table 3. The solid curves in figure 4 (a) and (b) show the predictions of the second order model with this final parameter set in comparison to the measured Σ_{EEC} and Σ_{AEEC} distributions at the hadron level: a good description is obtained for both distributions. This is emphasized in figure 4 (c) and (d), which shows the deviation of the model predictions with the data, defined as in figure 1 (c) and (d). For Σ_{AEEC}, the tuned model ERT-MC-2 always remains within one standard deviation of the data points, except for a small region between $\chi \approx 15°$ and $\chi \approx 28°$. For $y_{min} = 0.01$, as used in the Monte Carlo calculation, the transition between two- and three-jet production occurs for $\chi \approx 25°$, which perhaps explains the deviation from the data in this region.

The different values of $\Lambda_{\overline{MS}}$ found for the ERT-MC-1 and ERT-MC-2 parameter sets can be explained as follows. The second order Monte Carlo with the scale $\mu = M_{Z^0}$ for $\alpha_S(\mu)$ does not provide a good description of the two-jet region of global event shape variables in Z^0 hadronic decays, because the y_{min} value of 0.01 suppresses soft and colinear radiation relevant for this region. When the second order model is tuned using global event shapes and $< n_{ch.} >$ only (third column of tables 2 and 3), the two-jet region is emphasized because of its large bin statistics: the two-jet region contains little information about α_S and there is no reason to

[5] A recent measurement of this quantity by OPAL is $< n_{ch.} > = 21.4 \pm 0.4$ [27].

expect a meaningful result for $\Lambda_{\overline{MS}}$ since this region is not well described by the calculations. When $\Lambda_{\overline{MS}}$ is fit using the energy correlation asymmetry (fourth column of tables 2 and 3), a different value of $\Lambda_{\overline{MS}}$ is obtained: this second value is more meaningful because it is based on a variable which is sensitive to gluon radiation and yields a good description of that variable. From figure 3 it is seen that the experimental measurement, given by the corrected Σ_{AEEC} distribution integrated from 30° to 90°, is quite insensitive to the value of $\Lambda_{\overline{MS}}$ used to calculate the correction, i.e. the data points labeled (1), (2) and (3) are all consistent with each other to within their errors. This is a necessary condition in order for this method based on the second order Monte Carlo to be sensible.

4.3 Scale uncertainty and other theoretical errors

There are two additional sources of systematic uncertainty which we consider before summarizing our result for α_S. Both these errors are of theoretical origin: (1) disagreements between the results of different theoretical groups for the second order coefficient of Σ_{AEEC} and (2) the dependence of α_S on the choice of the renormalization scale.

Besides the Kunszt-Nason calculation, other second order calculations have been presented for the energy-energy correlation asymmetry. The different theoretical predictions for the second order coefficient are not in complete agreement with each other, as was pointed out in our earlier study [3]. The reasons for this lack of agreement are not well understood. Shown in figure 2 in comparison to the Kunszt-Nason result are the results of Falck and Kramer [23] and of Richards, Stirling and Ellis [24]. The Richards et al. result, like the Kunszt-Nason one, is valid for $y_{min} = 0$. Falck and Kramer introduce a definition for jets before calculating the energy correlation distributions: for the Falck-Kramer curve shown in figure 2, $y_{min} = 0.0001$. Since this y_{min} value is small, corresponding to a parton virtual mass of $Q_0 \approx 1$ GeV/c^2, it may be compared directly to the other calculations and to our data in figure 2. In [3], we also considered the second order calculation of Ali and Barreiro [29]. The Ali-Barreiro result was found to be intermediate to the Kunszt-Nason and Richards et al. ones and so we do not explicitly include it here. In figure 3 we show the Falck-Kramer result, in this case valid for $y_{min} = 0.01$, in comparison to the ERT Monte Carlo calculation which uses this same y_{min} value. The analytic calculations shown in figures 2 and 3 were all normalized to the first order total cross section σ_1, given by $\sigma_1 = \sigma_0(1+\alpha_S(M_{Z^0})/\pi)$, where σ_0 is the Born level cross section for hadronic production in e^+e^- annihilations.

The Falck-Kramer curve in figure 2 yields $\Lambda_{\overline{MS}} = 200 \pm 8$ MeV; the Richards et al. curve yields $\Lambda_{\overline{MS}} = 275 \pm 11$ MeV (statistical errors only). These differ by -20 MeV and +55 MeV, respectively, from the result obtained using the Kunszt-Nason formula. A smaller difference of about 15 MeV is obtained between the two theoretical curves which use $y_{min} = 0.01$, shown in figure 3. We therefore define

6. an error on $\Lambda_{\overline{MS}}$ of $+55$ MeV and -20 MeV, to be the uncertainty of $\Lambda_{\overline{MS}}$ due to disagreement between different second order theoretical calculations.

This is a relatively large error compared to the other uncertainties.

If the exact perturbative expression for Σ_{AEEC} were available to all orders, the α_S result would be independent of the choice of the renormalization scale μ. Since the theory is available up to second order only, a scale dependence can, in principle, be present. The solid curve in figure 5 (a) shows the $\Lambda_{\overline{MS}}$ value which is derived from the Kunszt-Nason formula as the value of the renormalization scale variable $x_\mu \equiv \mu/E_{c.m.}$ is changed from $x_\mu = 1$ to $x_\mu = 0.08$. The result for $x_\mu = 1$ corresponds to the analysis presented in section 4.1; the $\Lambda_{\overline{MS}}$ values shown for other choices of x_μ are obtained by repeating the analysis of figure 2 using different scales. The resulting χ^2 per degree of freedom (DOF) between data and theory is indicated at selected points along this curve by numerical values. These χ^2 values are calculated using the measured, differential Σ_{AEEC} distribution, corrected for hadronization using the parton shower in the angular range between 30° and 90°: not all bin-by-bin systematic errors have been included for the χ^2 calculation, which explains the relatively large values for χ^2/DOF. It is seen that the quality of the fit, as measured by the χ^2/DOF, remains essentially unchanged for $0.2 < x_\mu < 1.0$: the fit value of $\Lambda_{\overline{MS}}$ varies between 220 and 175 MeV in this range. We do not consider values of x_μ smaller than about 0.2 because of the larger χ^2/DOF. We therefore define

7. an error on $\Lambda_{\overline{MS}}$ of -45 MeV, given by the maximum deviation of $\Lambda_{\overline{MS}}$ which is observed for changes in the scale between $0.2 < x_\mu < 1.0$, relative to the result found for $x_\mu = 1$,

to be the uncertainty of $\Lambda_{\overline{MS}}$ due to the dependence on the choice of the scale μ. This dependence of $\Lambda_{\overline{MS}}$ on the choice of the renormalization scale is considerably smaller than what is observed for other variables, such as the jet rates, using this same second order theory (see e.g. [25, 26]).

In figure 5 (a), we include the results obtained with the Falck-Kramer, Richards et al. and ERT Monte Carlo calculations for the fitted value of $\Lambda_{\overline{MS}}$ as the renormalization scale is changed. The Falck-Kramer results are shown for both $y_{min} = 0.01$ and $y_{min} = 0.0001$. All of the analytic calculations exhibit the same behavior as was noted above for the Kunszt-Nason formula. The Monte Carlo calculation resembles these analytic results for values of x_μ larger than about 0.15. For values of x_μ smaller than about 0.15, its fitted value of $\Lambda_{\overline{MS}}$ decreases monotonically with x_μ, however. The reason for the anomalous behavior of the Monte Carlo calculation is discussed in the next section; following this we summarize our final result for α_S.

4.4 The second order ERT calculation in Jetset for small scale values

To second order, the Σ_{AEEC} distribution receives contributions from three- and four-parton jet states. The four-jet cross section is present at leading order only and is positive in all regions of phase space. The three-jet cross section has both leading and next-to-leading order terms, which for a given y_{min} value can be opposite in sign: therefore the differential three-jet cross section can be negative in some regions of phase space. A negative value of the matrix element implies that there are important missing higher order corrections: were the theory available to all orders, the differential cross section would be positive everywhere. As the value of the renormalization scale is varied, the relative importance of the leading and next-to-leading order

terms changes, so that a large portion of the three-jet cross section could, in principle, be negative for certain choices of the scale. These considerations apply equally to analytic and Monte Carlo calculations. The Monte Carlo result is unreliable if the matrix element is negative, however, because the matrix element is interpreted to be a probability for event generation in the Monte Carlo method. In the ERT Monte Carlo calculation in Jetset, the contribution from the region with negative cross section is ignored. The contribution from the region with positive cross section is then rescaled by a constant factor to conserve the overall three-jet rate [28].

To understand the anomalous behavior of the Monte Carlo curve shown in figure 5 (a) for scale values smaller than $x_\mu \approx 0.15$, we therefore examined its three- and four-parton jet cross sections for different choices of the scale.[6] We discovered that with $y_{min} = 0.01$ and $\Lambda_{\overline{MS}} \approx 200$ MeV, as in our analysis, the differential three-jet matrix element could be negative in a substantial region of phase space. The solid curve in figure 5 (b) shows the value of the three-jet matrix element, integrated over the region of phase space where it is negative, divided by the integral over the region where it is positive, as a function of the scale factor x_μ. In the notation used in this figure, M_3 denotes the differential three-jet cross section while Ω^- and Ω^+ are the phase space regions with negative and positive values of M_3, respectively. The ERT Monte Carlo in Jetset with $y_{min} = 0.01$ and $\Lambda_{\overline{MS}} = 200$ MeV was used to obtain this curve; similar results can be expected from the analytic formulae. It is seen that there is a finite region with negative three-jet cross section even for $x_\mu = 1$: the region with negative cross section contributes about 1% of the total three-jet rate in this case. For $x_\mu \approx 0.04$, this fraction has risen to be about 15%.

The dashed curve in figure 5 (b) shows the value of the energy correlation asymmetry, denoted A, after it is weighted by the matrix element M_3 and integrated over the region where M_3 is negative, divided by the corresponding quantity from the region where M_3 is positive. Thus this ratio shows the relative contribution of the regions with $M_3 < 0$ and $M_3 > 0$ to the overall asymmetry value. For both the numerator and the denominator, A is given by the integral of the Σ_{AEEC} distribution between 30° and 90° as for the rest of our analysis. For values of x_μ larger than about 0.15, the region with negative cross section contributes less than 10^{-2} to the total three-jet asymmetry, as shown: it can be expected that the analytic and Monte Carlo results would be in agreement for this region. For values of x_μ smaller than about 0.15, the relative contribution from the region with negative cross section is large, however: the analytic and Monte Carlo calculations can be expected to disagree in this case, since the asymmetry for $M_3 < 0$ is ignored in the Monte Carlo treatment as noted above. We have also checked the contribution of the four-jet cross section for different values of the scale. With $x_\mu \approx 0.04$, for example, we find the total asymmetry value from the Monte Carlo, given by the sum of the three- and four-jet contributions, to be about a factor of three larger than the analogous result which includes the region with $M_3 < 0$. This explains why the Monte Carlo fits the data with a very small value of $\Lambda_{\overline{MS}}$ relative to the analytic calculations, for values of x_μ smaller than about 0.15. We thus conclude that the anomalous behavior of the Monte Carlo curve shown in figure 5 (a) for small scale values is because of its inappropriate handling of the negative three-jet cross section and that the Monte Carlo calculation of Σ_{AEEC} is not reliable for values of x_μ smaller than about 0.15, if y_{min} is used at its recommended value [20] of 0.01.

Despite this problem which precludes its use for quantitative studies of α_S under the condi-

[6] We thank T. Sjöstrand for his help in the analysis presented in the remainder of this section.

tions noted above, the ERT Monte Carlo in Jetset with a small scale value is found to provide a good general parameterization of the Z^0 hadronic decay data when used in conjunction with a string hadronization model. This is discussed in the appendix.

4.5 Final result for α_S

Our final result for $\Lambda_{\overline{MS}}$ is

$$\begin{aligned} \Lambda_{\overline{MS}} &= 220 \pm 9\,(\text{stat.}) \pm 32\,(\text{exp.syst.})\,^{+132}_{-50}\,(\text{theor.syst.})\ \text{MeV} \\ &= 220\,^{+136}_{-60}\ \text{MeV}\ . \end{aligned}$$

The value of 220 MeV and its statistical error are taken from item 1 in section 4.1. The experimental systematic error is defined by adding items 2 and 4 in section 4.1 in quadrature. The theoretical systematic error is given by item 3 in section 4.1, added in quadrature with item 5 in section 4.2 and item 7 in section 4.3. This value of $\Lambda_{\overline{MS}}$ is equivalent to [22]

$$\begin{aligned} \alpha_S(M_{Z^0}) &= 0.118 \pm 0.001\,(\text{stat.}) \pm 0.003\,(\text{exp.syst.})\,^{+0.009}_{-0.004}\,(\text{theor.syst.}) \\ &= 0.118\,^{+0.009}_{-0.005}\ , \end{aligned}$$

so that the accuracy of our α_S measurement is 5.5%. The largest uncertainty is the theoretical one due to the unknown higher order terms. For this final result, we have not included the discrepancy between the different theoretical calculations, given by item 6 in section 4.3, so as to allow our result to be better compared to other experiments [4, 5, 30]. If this last error is included in quadrature, we obtain $\Lambda_{\overline{MS}} = 220\,^{+147}_{-63}$ MeV or $\alpha_S(M_{Z^0}) = 0.118\,^{+0.010}_{-0.006}$, which represents an α_S measurement with 6.8% accuracy. In our previous study of the energy correlation asymmetry, we obtained $\alpha_S(M_{Z^0}) = 0.117 \pm 0.009$ [3]. The smaller error for the present work is due to reduced statistical and experimental systematic uncertainties. The result presented here is also more precise than the α_S result we obtained using jet rates, which was $\alpha_S(M_{Z^0}) = 0.118 \pm 0.008$ [26]. All these α_S results are fully consistent with each other: the difference between the measurements is much smaller than their quoted errors because of common systematic uncertainties.

5 Summary and conclusions

In this letter we have presented an analysis of energy correlations in hadronic Z^0 decays, performed by the OPAL Collaboration. From the asymmetry in the energy-energy correlation function, we obtain

$$\Lambda_{\overline{MS}} = 220\,^{+136}_{-60}\ \text{MeV}$$

and

$$\alpha_S(M_{Z^0}) = 0.118\,^{+0.009}_{-0.005}\ ,$$

for the scale parameter and coupling constant of strong interactions, respectively, evaluated at the Z^0 peak. This measurement represents a more precise result than our previously published measurements of α_S, using energy correlations [3] and jet rates [26], while being fully consistent with these earlier studies. This updated measurement is also consistent with the α_S results

obtained by other experiments at the Z^0 energy [5, 6, 30]. The main source of error for our final result is the uncertainty due to the unknown, higher than second order corrections. Therefore a reduction in the error of α_S from energy correlations, at the Z^0 energy, will most likely require the incorporation of new theoretical elements such as extensions to the second order theory. The second largest source of error (not included in the final result) is the disagreement between different second order calculations for the next-to-leading order term.

As a by-product of the α_S measurement, we have examined the predictions of the second order ERT calculation in the Jetset Monte Carlo. This calculation is found to yield a negative three-jet matrix element in a substantial region of phase space, if a small value of the renormalization scale is used in conjunction with $y_{min} = 0.01$ to define resolvable jets. For the energy correlation asymmetry, the α_S result is reliable only for scale values larger than about $\mu = 0.15 \cdot E_{c.m.}$, if $y_{min} = 0.01$. For smaller values of the scale in the generator, the extracted value of α_S will be biased towards a lower result.

6 Acknowledgements

We thank Torbjörn Sjöstrand for his help in understanding the second order ERT calculation in Jetset. We also thank the SL Division for the efficient operation of the LEP accelerator and their continuing close cooperation with our experimental group. In addition to the support staff at our own institutions we are pleased to acknowledge the
Department of Energy, USA,

National Science Foundation, USA,
Science and Engineering Research Council, UK,
Natural Sciences and Engineering Research Council,Canada,
Israeli Ministry of Science,
Minerva Gesellschaft,
Japanese Ministry of Education, Science and Culture (the Monbusho) and a grant under the Monbusho International Science Research Program,
American Israeli Bi-national Science Foundation,
Direction des Sciences de la Matière du Commissariat à l'Energie Atomique, France,
Bundesministerium für Forschung und Technologie, FRG,
A.P. Sloan Foundation and Junta Nacional de Investigação Científica e Tecnológica, Portugal.

Appendix: Event shape description by the ERT Monte Carlo with a small scale value

For the second order Monte Carlo discussed in section 4.2, a renormalization scale value $\mu = M_{Z^0}$ was chosen for the argument of $\alpha_S(\mu)$. Such a model does not provide a good description of the two-jet region of global event shape variables in hadronic Z^0 decays, however, as was mentioned in section 4.2; also the four-jet rate is underestimated by such a model if α_S is derived from the three-jet rate [31].[7] These features suggest that there are important higher order terms which are missing from the event shape and jet rate calculations. One approach to possibly minimize the importance of the unknown higher order terms is to use a small value for the renormalization scale μ. It is interesting to see how well a second order Monte Carlo with a small value of the scale μ can reproduce the global properties of multihadronic Z^0 decays including the energy correlation data.

The second order ERT model in Jetset was therefore retuned using the procedure discussed in section 4.2, with the scale value $x_\mu \equiv \mu/E_{c.m.} = 0.0447$: this is the default value in Jetset if an optimized scale is selected. Again, we employed the recommended y_{min} value of 0.01 [20]. The value of $\Lambda_{\overline{MS}}$ was obtained by fitting to the integral of the corrected Σ_{AEEC} distribution, as in figure 3, with hadronization corrections calculated from the Monte Carlo with the optimized scale. An iterative procedure identical to that presented in figure 3 was employed. The parameter values obtained are listed in the fifth column of table 2: this parameter set is denoted ERT-MC-3. The resulting value of $< n_{ch.} >$ and the χ^2 values with the global event shape data from [13] are given in the fifth column of table 3. A much better overall description of the data is obtained relative to the model for which $x_\mu = 1$ (ERT-MC-2). The overall χ^2 value for 109 bins of data drops from about 2200 for $x_\mu = 1$ to 399 for $x_\mu = 0.0447$, as shown in table 3. This decrease in the overall χ^2 value is primarily due to a better description of the two- and four-jet event regions. The predictions of the ERT-MC-3 model for the energy correlation data are shown in figure 4 by the dashed lines: in contrast to the case of the global event shape variables, about an equally good description is obtained both for this model and for that with $x_\mu = 1$ (solid lines), as is more clearly visible from figure 4 (c) and (d). We include in figure 4 and in table 3 the results obtained from the same second order ERT Monte Carlo in Jetset, using the parameter set of de Boer, Fürstenau and Köhne [32] (ERT-MC-BFK) which also employs $y_{min} = 0.01$ and $x_\mu = 0.0447$. We do not obtain as good a description of the multihadronic Z^0 decay data as we do using the ERT-MC-3 set presented above.

The interpretation of the good description of data obtained with the ERT-MC-3 parameter set is not completely clear, given that the three-jet matrix element is negative in a substantial region of phase space for this model (cf. the points indicated by stars in figure 5 (b)). The $\Lambda_{\overline{MS}}$ result obtained with this calculation is, as a consequence, biased toward low values: for $x_\mu = 0.0447$ we obtain $\Lambda_{\overline{MS}} = 150$ MeV from the Monte Carlo curve in figure 5 (a) (compared to $\Lambda_{\overline{MS}} = 130$ MeV for the ERT-MC-3 parameter set), which is smaller than the lower limit permitted by our measurement (section 4.5). We note that this low value is very similar to the results published in [4] and [5] which are based on the same ERT Monte Carlo with $x_\mu = 0.0447$ and $y_{min} = 0.01$. The ERT-MC-3 model nonetheless provides a good general parameterization of the data. Parton shower models such as Jetset, Herwig and Cojets yield overall χ^2 values

[7] These aspects are not very important for our α_S study since the Σ_{AEEC} distribution is dominated by three-jet events for $\mu = M_{Z^0}$.

for the distributions listed in table 3 which are two to three times smaller [13, 16] than what is obtained for the ERT-MC-3 model, however.

References

[1] C.L. Basham et al., Phys. Rev. Lett. 41 (1978) 1585; Phys. Rev. D17 (1978) 2298.

[2] MARK2 Collab., D. Schlatter et al., Phys. Rev. Lett. 49 (1982) 521;
PLUTO Collab., Ch. Berger et al., Z. Phys. C12 (1982) 297;
CELLO Collab., H-J. Behrend et al., Z. Phys. C14 (1982) 95;
MARKJ Collab., B. Adeva et al., Phys. Rev. Lett. 50 (1983) 2051;
JADE Collab., W. Bartel et al., Z. Phys. C25 (1984) 231;
CELLO Collab., H.J. Behrend et al., Phys. Lett. 138B (1984) 311;
TASSO Collab., M. Althoff et al., Z. Phys. C26 (1984) 157;
MAC Collab., E. Fernandez et al., Phys. Rev. D31 (1985) 2724;
MARKJ Collab., B. Adeva et al., Phys. Rev. Lett. 54 (1985) 1750;
TASSO Collab., W. Braunschweig et al., Z. Phys. C36 (1987) 349;
MARK2 Collab., D.R. Wood et al., Phys. Rev. D37 (1988) 3091;
TOPAZ Collab., I. Adachi et al., Phys. Lett. B227 (1989) 495.

[3] OPAL Collab., M.Z. Akrawy et al., Phys. Lett. B252 (1990) 159.

[4] DELPHI Collab., P. Abreu et al., Phys. Lett. B252 (1990) 149.

[5] DELPHI Collab., P. Abreu et al., CERN-PPE/91-181.

[6] L3 Collab., B. Adeva et al., Phys. Lett. B257 (1991) 469.

[7] Z. Kunszt, P. Nason, G. Marchesini and B.R. Webber, "QCD" in "Z Physics at LEP 1", CERN 89-08, vol. 1, eds. G. Altarelli, R. Kleiss and C. Verzegnassi (Geneva 1989).

[8] OPAL Collab., K. Ahmet et al., Nucl. Inst. and Methods A305 (1991) 275.

[9] M. Arignon et al., CERN-PPE/91-32 (1991), submitted to Nucl. Inst. and Methods.

[10] OPAL Collab., G. Alexander et al., Z. Phys. C52 (1991) 175.

[11] T. Sjöstrand, Comp. Phys. Comm. 47 (1987) 347;
T. Sjöstrand and M. Bengtsson, Comp. Phys. Comm. 43 (1987) 367.

[12] J. Allison *et al.*, Comp. Phys. Comm. 47 (1987) 55;
D. R. Ward, Proc. MC'91 Workshop, NIKHEF, Amsterdam, 1991.

[13] OPAL Collab., M.Z. Akrawy et al., Z. Phys. C47 (1990) 505.

[14] G. Marchesini and B.R. Webber, Nucl. Phys. B310 (1988) 464;
G. Marchesini, B.R. Webber et al., Cavendish-HEP-91-26.

[15] R. Odorico, Comp. Phys. Comm. 32 (1984) 139; Comp. Phys. Comm. 59 (1990) 527.

[16] P. Mazzanti and R. Odorico, Bologna preprint DDFUB 91/4 (1991).

[17] OPAL Collab., M.Z. Akrawy et al., Phys. Lett. B261 (1991) 334.

[18] OPAL Collab., G. Alexander et al., Phys. Lett. B265 (1991) 462.

[19] R.K. Ellis, D.A. Ross and A.E. Terrano, Phys. Rev. Lett. 45 (1980) 1226; Nucl. Phys. B178 (1981) 421;
R.-y. Zhu, MIT Ph.D. Thesis, MIT-LNS report RX-1033 (1983).

[20] T. Sjöstrand et al., "QCD Generators" in "Z Physics at LEP 1", CERN 89-08, vol. 3, eds. G. Altarelli, R. Kleiss and C. Verzegnassi (Geneva 1989).

[21] M. Chen and L. Garrido, Phys. Lett. B180 (1986) 409.

[22] Review of Particle Properties, Phys. Lett. B239 (1990).

[23] N.K. Falck and G. Kramer, Z. Phys. C42 (1989) 459.

[24] D.G. Richards, W.J. Stirling and S.D. Ellis, Phys. Lett. 199B (1982) 193; Nucl. Phys. B229 (1983) 317.

[25] N. Magnoli, P. Nason and R. Rattazzi, Phys. Lett. B252 (1990) 271.

[26] OPAL Collab., M.Z. Akrawy et al., Phys. Lett. B235 (1990) 389; Z. Phys. C49 (1991) 375.

[27] OPAL Collab., P.D. Acton et al., CERN-PPE/91-176, submitted to Z. Phys. C.

[28] T. Sjöstrand, private communication.

[29] A. Ali and F. Barreiro, Phys. Lett. 118B (1982) 155; Nucl. Phys. B236 (1984) 269.

[30] MARK2 Collab., S. Komamiya et al., Phys. Rev. Lett. 64 (1990) 987;
DELPHI Collab., P. Abreu et al., Phys. Lett. B247 (1990) 167;
L3 Collab., B. Adeva et al., Phys. Lett. B248 (1991) 464;
ALEPH Collab., D. Decamp et al., Phys. Lett. B257 (1991) 479; Phys. Lett. B255 (1991) 623.

[31] JADE Collab., W. Bartel et al., Z. Phys. C33 (1986) 23.

[32] W. de Boer, H. Fürstenau and J.H. Köhne, Z. Phys. C49 (1991) 141.

Bin	χ (deg.)	$\Sigma_{EEC}(\chi)(\mathrm{rad.}^{-1})$	$\Sigma_{EEC}(180^\circ - \chi)(\mathrm{rad}^{-1})$	$\Sigma_{AEEC}(\mathrm{rad.}^{-1})$
1	0-1	4.646 ± 0.181	0.255 ± 0.019	-4.391 ± 0.165
2	1-2	0.933 ± 0.220	0.710 ± 0.080	-0.223 ± 0.141
3	2-3	1.289 ± 0.088	1.038 ± 0.047	-0.251 ± 0.132
4	3-4	1.383 ± 0.169	1.216 ± 0.093	-0.167 ± 0.261
5	4-5	1.340 ± 0.157	1.284 ± 0.058	-0.0565± 0.212
6	5-6	1.258 ± 0.087	1.296 ± 0.047	0.0376± 0.133
7	6-7	1.149 ± 0.058	1.273 ± 0.026	0.124 ± 0.083
8	7-8	1.037 ± 0.035	1.209 ± 0.012	0.172 ± 0.044
9	8-9	0.933 ± 0.021	1.146 ± 0.010	0.213 ± 0.017
10	9-10	0.839 ± 0.022	1.064 ± 0.006	0.225 ± 0.022
11	10-11	0.758 ± 0.025	0.994 ± 0.016	0.236 ± 0.016
12	11-12	0.690 ± 0.020	0.922 ± 0.017	0.231 ± 0.020
13	12-13	0.626 ± 0.014	0.8519 ± 0.0056	0.225 ± 0.010
14	13-14	0.568 ± 0.013	0.786 ± 0.022	0.218 ± 0.012
15	14-15	0.5193± 0.0092	0.734 ± 0.019	0.215 ± 0.012
16	15-16	0.4732± 0.0045	0.684 ± 0.016	0.211 ± 0.012
17	16-17	0.433 ± 0.012	0.631 ± 0.011	0.1983± 0.0065
18	17-18	0.396 ± 0.014	0.5864 ± 0.0088	0.1899± 0.0067
19	18-19	0.3662± 0.0095	0.5455 ± 0.0083	0.1792± 0.0038
20	19-20	0.3367± 0.0051	0.5094 ± 0.0046	0.1727± 0.0040
21	20-21	0.3103± 0.0064	0.4724 ± 0.0064	0.1621± 0.0024
22	21-22	0.288 ± 0.011	0.444 ± 0.013	0.1563± 0.0041
23	22-23	0.2690± 0.0073	0.421 ± 0.014	0.1519± 0.0075
24	23-24	0.2526± 0.0054	0.394 ± 0.012	0.1410± 0.0074
25	24-25	0.2372± 0.0057	0.3694 ± 0.0086	0.1322± 0.0057
26	25-26	0.2239± 0.0088	0.3509 ± 0.0090	0.1271± 0.0028
27	26-27	0.2119± 0.0044	0.3317 ± 0.0072	0.1198± 0.0039
28	27-28	0.2011± 0.0024	0.3128 ± 0.0055	0.1117± 0.0035
29	28-29	0.1927± 0.0038	0.2982 ± 0.0061	0.1055± 0.0044
30	29-30	0.1835± 0.0035	0.2827 ± 0.0056	0.0992± 0.0028

Table 1: The EEC and AEEC distributions from Z^0 hadronic decays, at the hadron level, unfolded for initial-state radiation and for detector acceptance and resolution. The errors include the full statistical and systematic uncertainties.

Bin	χ (deg.)	$\Sigma_{EEC}(\chi)(\text{rad.}^{-1})$	$\Sigma_{EEC}(180^\circ - \chi)(\text{rad}^{-1})$	$\Sigma_{AEEC}(\text{rad.}^{-1})$
31	30-31	0.1753± 0.0020	0.2693 ± 0.0036	0.0940± 0.0034
32	31-32	0.1678± 0.0024	0.2546 ± 0.0032	0.0868± 0.0030
33	32-33	0.1617± 0.0025	0.2428 ± 0.0038	0.0811± 0.0035
34	33-34	0.1564± 0.0030	0.2356 ± 0.0031	0.0792± 0.0042
35	34-35	0.1494± 0.0017	0.2260 ± 0.0047	0.0766± 0.0048
36	35-36	0.1447± 0.0013	0.2157 ± 0.0031	0.0711± 0.0032
37	36-37	0.1409± 0.0030	0.2080 ± 0.0014	0.0672± 0.0035
38	37-38	0.1367± 0.0012	0.1992 ± 0.0023	0.0624± 0.0018
39	38-39	0.1316± 0.0021	0.1903 ± 0.0023	0.0587± 0.0021
40	39-40	0.1281± 0.0011	0.1856 ± 0.0012	0.0575± 0.0016
41	40-41	0.1261± 0.0013	0.1781 ± 0.0010	0.0520± 0.0018
42	41-42	0.1224± 0.0023	0.1721 ± 0.0027	0.0498± 0.0019
43	42-43	0.1191± 0.0021	0.1669 ± 0.0013	0.0477± 0.0025
44	43-44	0.1160± 0.0019	0.1621 ± 0.0019	0.0461± 0.0023
45	44-45	0.1133± 0.0009	0.1557 ± 0.0026	0.0425± 0.0032
46	45-46	0.1103± 0.0021	0.1513 ± 0.0014	0.0410± 0.0026
47	46-47	0.1091± 0.0024	0.1467 ± 0.0038	0.0376± 0.0030
48	47-48	0.1058± 0.0016	0.1417 ± 0.0017	0.0360± 0.0017
49	48-49	0.1048± 0.0025	0.1400 ± 0.0015	0.0352± 0.0029
50	49-50	0.1029± 0.0019	0.1360 ± 0.0015	0.0331± 0.0016
51	50-51	0.1001± 0.0014	0.1313 ± 0.0055	0.0312± 0.0017
52	51-52	0.0992± 0.0015	0.1275 ± 0.0040	0.0284± 0.0025
53	52-53	0.0965± 0.0009	0.1247 ± 0.0012	0.0282± 0.0012
54	53-54	0.0956± 0.0013	0.1233 ± 0.0035	0.0277± 0.0023
55	54-55	0.0937± 0.0013	0.1189 ± 0.0019	0.0252± 0.0031
56	55-56	0.0930± 0.0014	0.1175 ± 0.0017	0.0245± 0.0023
57	56-57	0.0918± 0.0009	0.1148 ± 0.0026	0.0230± 0.0011
58	57-58	0.0903± 0.0020	0.1121 ± 0.0016	0.0218± 0.0022
59	58-59	0.0892± 0.0017	0.1103 ± 0.0009	0.0211± 0.0022
60	59-60	0.0880± 0.0010	0.1073 ± 0.0008	0.0194± 0.0014

Table 1: continued.

Bin	χ (deg.)	$\Sigma_{EEC}(\chi)(\text{rad.}^{-1})$	$\Sigma_{EEC}(180^\circ - \chi)(\text{rad}^{-1})$	$\Sigma_{AEEC}(\text{rad.}^{-1})$
61	60-61	0.0869± 0.0019	0.1054 ± 0.0029	0.0185± 0.0011
62	61-62	0.0866± 0.0011	0.1050 ± 0.0029	0.0184± 0.0011
63	62-63	0.0852± 0.0010	0.1025 ± 0.0030	0.0173± 0.0013
64	63-64	0.0852± 0.0010	0.1013 ± 0.0021	0.0162± 0.0029
65	64-65	0.0840± 0.0013	0.0995 ± 0.0014	0.0156± 0.0015
66	65-66	0.0830± 0.0013	0.0965 ± 0.0023	0.0135± 0.0012
67	66-67	0.0822± 0.0013	0.0953 ± 0.0018	0.0132± 0.0013
68	67-68	0.0816± 0.0013	0.0935 ± 0.0038	0.0120± 0.0019
69	68-69	0.0813± 0.0010	0.0932 ± 0.0020	0.0120± 0.0010
70	69-70	0.0807± 0.0019	0.0919 ± 0.0015	0.0111± 0.0014
71	70-71	0.0797± 0.0010	0.0894 ± 0.0014	0.0097± 0.0019
72	71-72	0.0782± 0.0018	0.0892 ± 0.0021	0.0111± 0.0012
73	72-73	0.0788± 0.0023	0.0880 ± 0.0006	0.0093± 0.0009
74	73-74	0.0795± 0.0020	0.0882 ± 0.0010	0.0086± 0.0009
75	74-75	0.0786± 0.0024	0.0872 ± 0.0017	0.0086± 0.0012
76	75-76	0.0781± 0.0016	0.0866 ± 0.0015	0.0085± 0.0008
77	76-77	0.0783± 0.0008	0.0844 ± 0.0012	0.0061± 0.0012
78	77-78	0.0784± 0.0013	0.0842 ± 0.0012	0.0058± 0.0011
79	78-79	0.0770± 0.0008	0.0835 ± 0.0013	0.0065± 0.0009
80	79-80	0.0766± 0.0011	0.0823 ± 0.0012	0.0056± 0.0009
81	80-81	0.0777± 0.0019	0.0823 ± 0.0015	0.0046± 0.0009
82	81-82	0.0771± 0.0022	0.0802 ± 0.0006	0.0032± 0.0019
83	82-83	0.0774± 0.0017	0.0813 ± 0.0013	0.0040± 0.0009
84	83-84	0.0767± 0.0018	0.0807 ± 0.0023	0.0040± 0.0014
85	84-85	0.0764± 0.0007	0.0810 ± 0.0015	0.0046± 0.0011
86	85-86	0.0775± 0.0014	0.0798 ± 0.0029	0.0023± 0.0010
87	86-87	0.0775± 0.0019	0.0793 ± 0.0023	0.0018± 0.0011
88	87-88	0.0767± 0.0016	0.0785 ± 0.0019	0.0019± 0.0011
89	88-89	0.0780± 0.0024	0.0785 ± 0.0023	0.0005± 0.0015
90	89-90	0.0785± 0.0019	0.0785 ± 0.0012	0.0001± 0.0012

Table 1: continued.

Parameter	Name in Jetset Monte Carlo	ERT-MC-1 ($x_\mu = 1$) tuned to event shapes only	ERT-MC-2 ($x_\mu = 1$) tuned to event shapes and Σ_{AEEC}	ERT-MC-3 ($x_\mu = 0.0447$) tuned to event shapes and Σ_{AEEC}
$\Lambda_{\overline{MS}}$	PARJ(122)	0.28 GeV	0.35 GeV	0.13 GeV
σ_q	PARJ(21)	0.49 GeV	0.49 GeV	0.42 GeV
a	PARJ(41)	1.80	1.80	1.50
${x_\mu}^2$	PARJ(129)	1.0	1.0	0.002
y_{min}	PARJ(125)	0.01	0.01	0.01
b	PARJ(42)	0.6 GeV^{-2}	0.6 GeV^{-2}	0.6 GeV^{-2}

Table 2: The main parameters of the ERT second order Monte Carlo with Lund string hadronization, in Jetset version 7.2, which control the momentum distribution of hadrons. For the parameter set ERT-MC-1, $\Lambda_{\overline{MS}}$, σ_q and a were fit to global event shape distributions and the mean charged multiplicity $< n_{ch.} >$. For ERT-MC-2, $\Lambda_{\overline{MS}}$ was fixed to fit to the energy correlation asymmetry and then σ_q and a were fit as for ERT-MC-1. The parameter set ERT-MC-3 was obtained like ERT-MC-2, except that a small value was used for the renormalization scale variable x_μ. The three parameters x_μ, y_{min} and b were kept fixed at the values indicated.

Distribution	Nr. of bins	ERT-MC-1 ($x_\mu = 1$) tuned to event shapes only	ERT-MC-2 ($x_\mu = 1$) tuned to event shapes and Σ_{AEEC}	ERT-MC-3 ($x_\mu = 0.0447$) tuned to event shapes and Σ_{AEEC}	ERT-MC-BFK ($x_\mu = 0.0447$)
Thrust T	13	279.9	330.6	40.4	206.5
T_{minor}	13	305.3	289.9	67.1	44.6
T_{major}	10	112.7	143.7	72.1	91.5
Oblateness O	12	20.7	25.0	18.7	59.5
Sphericity S	17	159.4	216.9	60.4	76.3
Aplanarity A	17	252.2	247.5	54.1	55.9
D variable	16	255.0	342.4	31.1	94.0
(H_2/H_0)	11	464.9	591.7	55.0	315.7
Totals	109	1850	2188	399	944
$< n_{ch} >$		21.0 ± 0.02	21.1 ± 0.02	21.3 ± 0.02	21.8 ± 0.03

Table 3: The χ^2 values between measured event shape distributions from [13] and the optimized second order Monte Carlos. The mean charged multiplicity value $< n_{ch.} >$ from the models is also given. There are 50,000 events in each Monte Carlo sample.

Figure Captions

Figure 1. Measured (a) Σ_{EEC} and (b) Σ_{AEEC} distributions, at the hadron level, unfolded for detector acceptance and resolution and for initial-state photon radiation. The predictions of the Herwig and Cojets parton shower models are shown in comparison. The deviations of the model predictions from the measurements are shown in (c) and (d) for Σ_{EEC} and Σ_{AEEC}, respectively. The predictions of the Jetset parton shower model are included in these deviation plots. The standard deviation is defined using the full statistical and systematic errors of the data points. The hatched area indicates the region of plus and minus one standard deviation.

Figure 2 The values obtained for the measured $\Sigma_{AEEC}(\chi)$ distribution after it is corrected for hadronization and integrated from $\chi = 30°$ to $\chi = 90°$, using various parton shower models and data sets for the corrections, as indicated. Shown as a function of $\Lambda_{\overline{MS}}$ are the predictions of several second order analytic calculations for the Σ_{AEEC} distribution, integrated over the same interval.

Figure 3 The values obtained for the $\Sigma_{AEEC}(\chi)$ distribution, corrected for hadronization using a second order Monte Carlo and integrated from $\chi = 30°$ to $\chi = 90°$, with three different choices of $\Lambda_{\overline{MS}}$ to calculate the corrections as explained in the text. The theoretical predictions from the second order Monte Carlo and from an analytic calculation are shown, as a function of $\Lambda_{\overline{MS}}$.

Figure 4 The measured (a) Σ_{EEC} and (b) Σ_{AEEC} distributions, as in figure 1, in comparison to the second order ERT matrix element calculation in Jetset, followed by Lund string hadronization, for various parameter sets. The standard deviation plots for Σ_{EEC} and Σ_{AEEC}, shown in (c) and (d), respectively, are defined as in figure 1.

Figure5 (a) The measured value of $\Lambda_{\overline{MS}}$ obtained from various analytic and Monte Carlo calculations as the renormalization scale factor $x_\mu \equiv \mu / E_{c.m.}$ is changed. The number of flavors is $n_f = 5$. (b) The solid curve shows the magnitude of the three-jet matrix element from the ERT second order Monte Carlo in Jetset, integrated over the region of phase space where it is negative, divided by its magnitude integrated over the region where it is positive, as a function of x_μ. The dashed curve shows the analogous ratio, weighted by the value of the energy correlation asymmetry A, as is explained in the text. The stars show the values obtained for $x_\mu = 0.0447$ (see appendix).

Figure 1

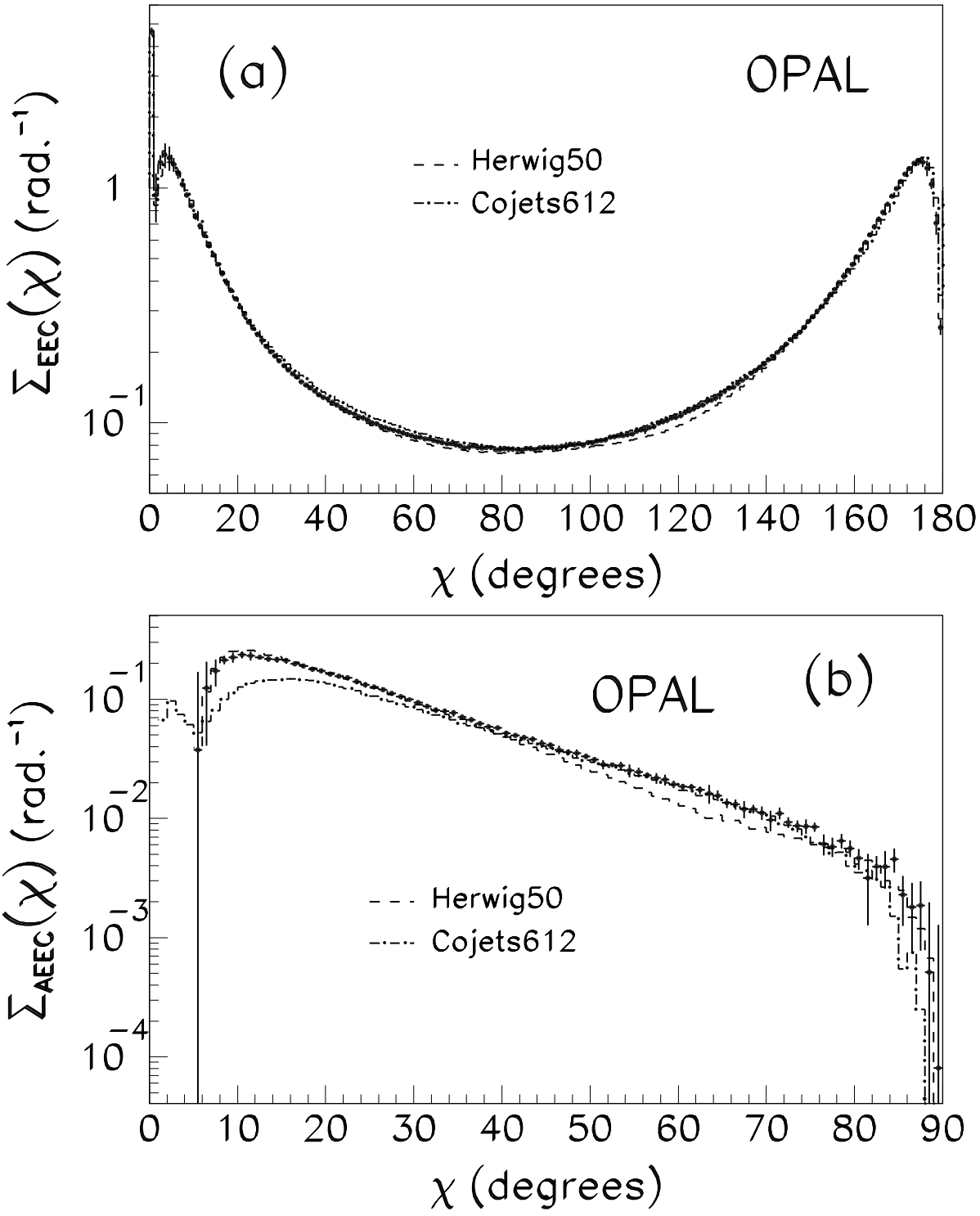
(a)
OPAL
Herwig50
Cojets612
$\Sigma_{EEC}(\chi)$ (rad.$^{-1}$)
1
10^{-1}
0 20 40 60 80 100 120 140 160 180
χ (degrees)
OPAL
(b)
Herwig50
Cojets612
$\Sigma_{AEEC}(\chi)$ (rad.$^{-1}$)
10^{-1}
10^{-2}
10^{-3}
10^{-4}
0 10 20 30 40 50 60 70 80 90
χ (degrees)

Figure 1

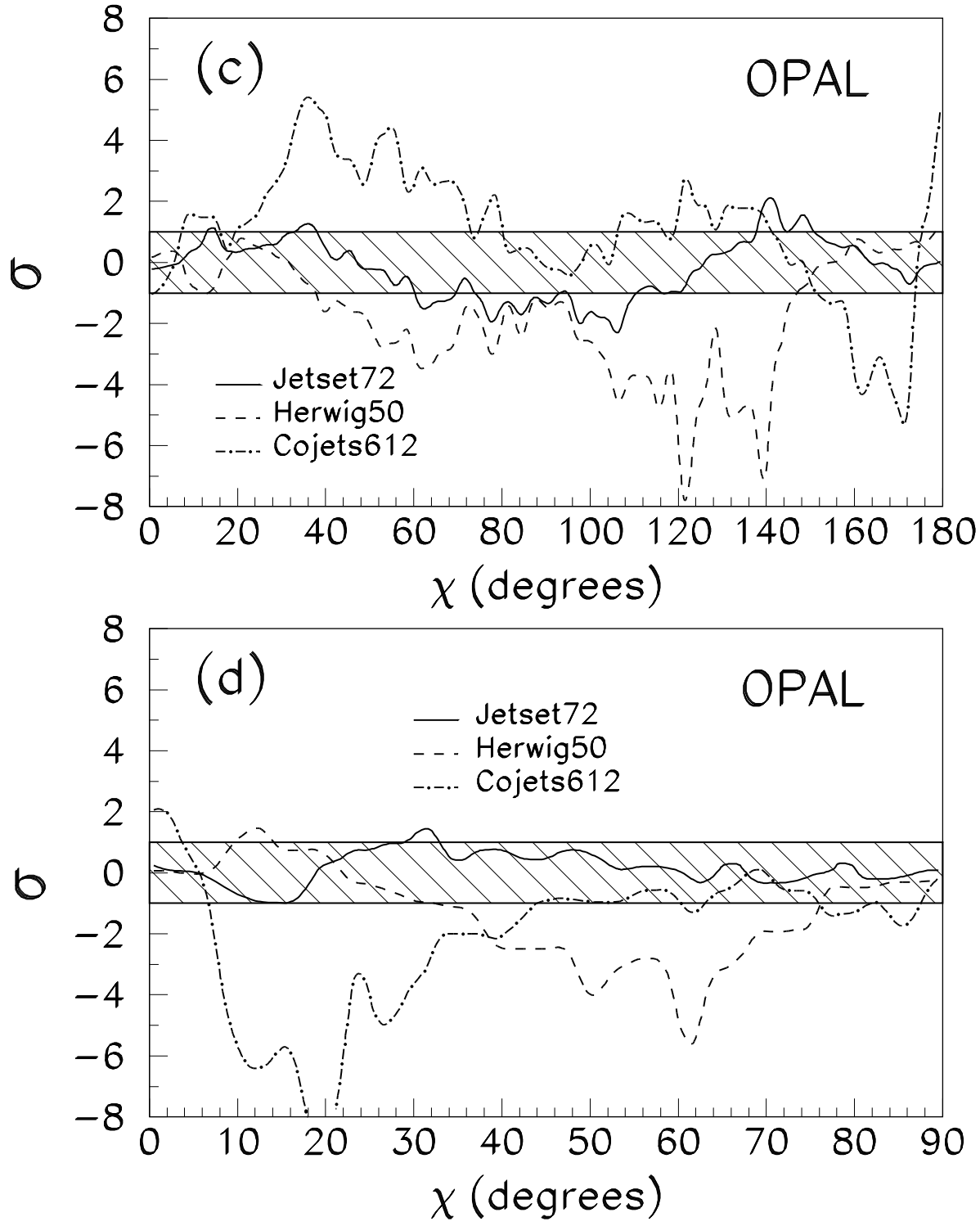
(c)
OPAL
Jetset72
Herwig50
Cojets612
σ
χ (degrees)
(d)
OPAL
Jetset72
Herwig50
Cojets612
σ
χ (degrees)

Figure 2

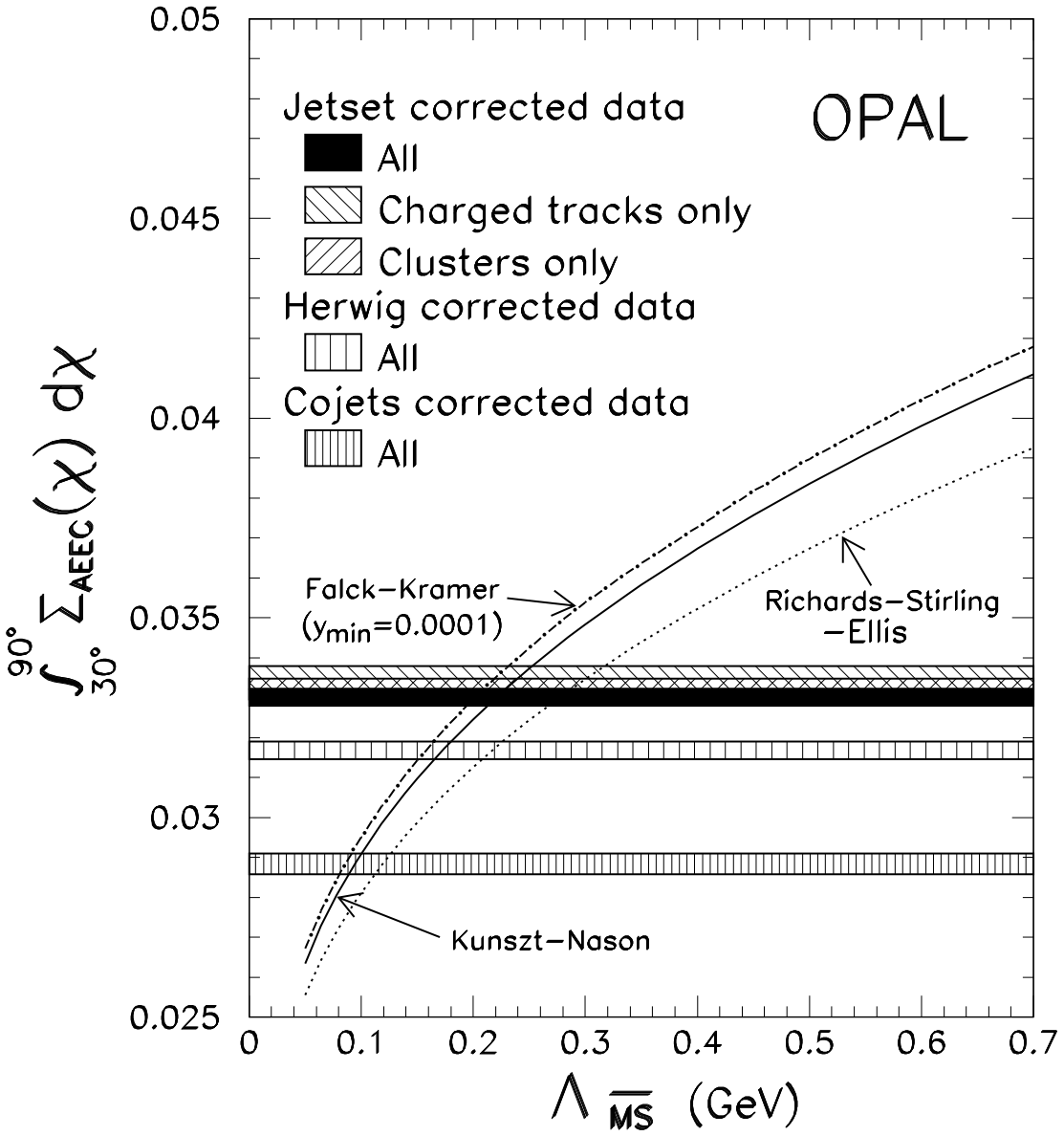
OPAL
Jetset corrected data
All
Charged tracks only
Clusters only
Herwig corrected data
All
Cojets corrected data
All
Falck−Kramer
(y_{min}=0.0001)
Richards−Stirling
−Ellis
Kunszt−Nason
$\int_{30°}^{90°} \Sigma_{AEEC}(\chi)\, d\chi$
$\Lambda_{\overline{MS}}$ (GeV)
0.05
0.045
0.04
0.035
0.03
0.025
0
0.1
0.2
0.3
0.4
0.5
0.6
0.7

Figure 3

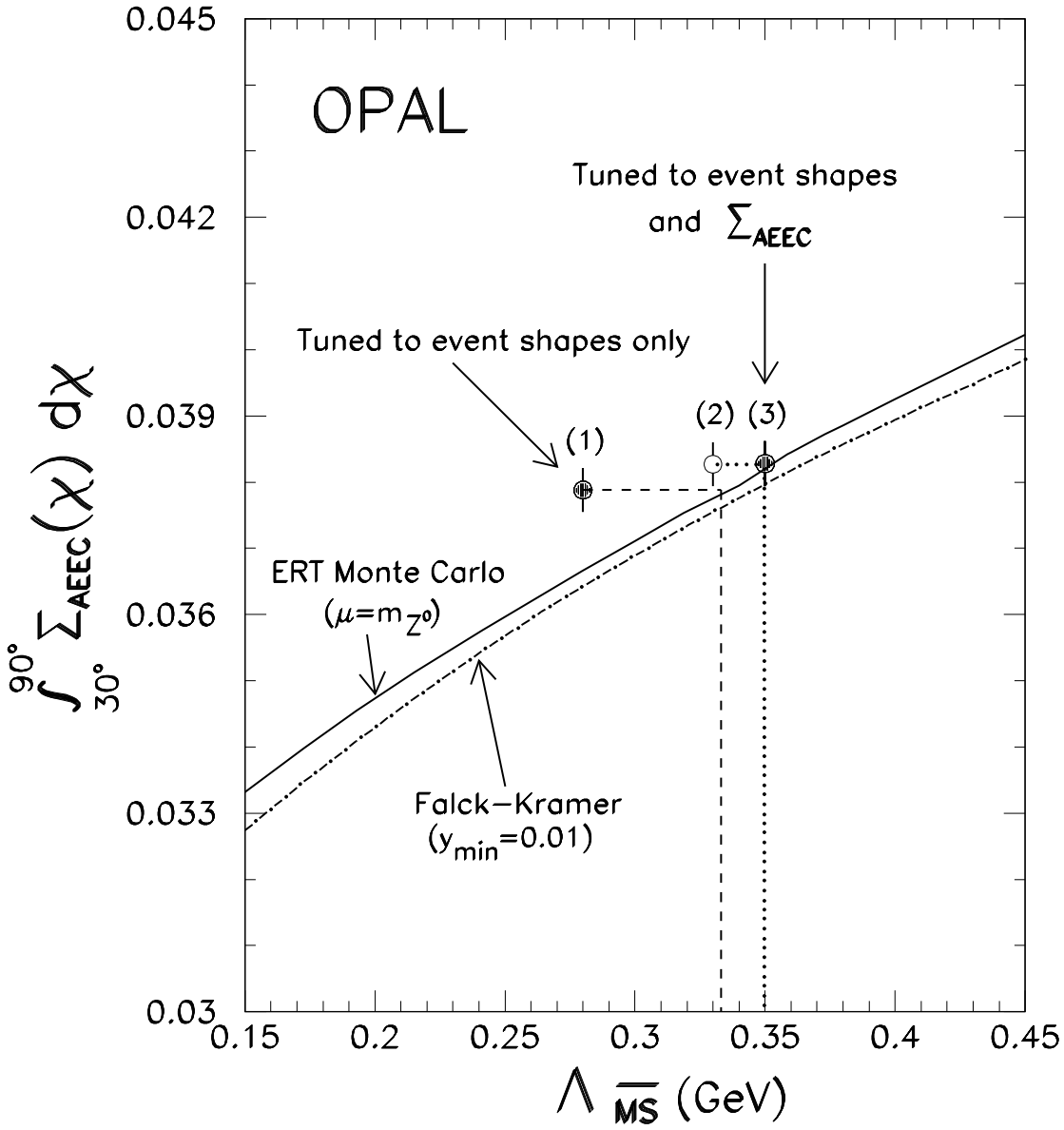
OPAL
Tuned to event shapes
and Σ_{AEEC}
Tuned to event shapes only
(1)
(2) (3)
ERT Monte Carlo
($\mu=m_{Z^0}$)
Falck−Kramer
($y_{min}=0.01$)
$\int_{30°}^{90°} \Sigma_{AEEC}(\chi)\, d\chi$
$\Lambda_{\overline{MS}}$ (GeV)
0.045
0.042
0.039
0.036
0.033
0.03
0.15
0.2
0.25
0.3
0.35
0.4
0.45

Figure 4

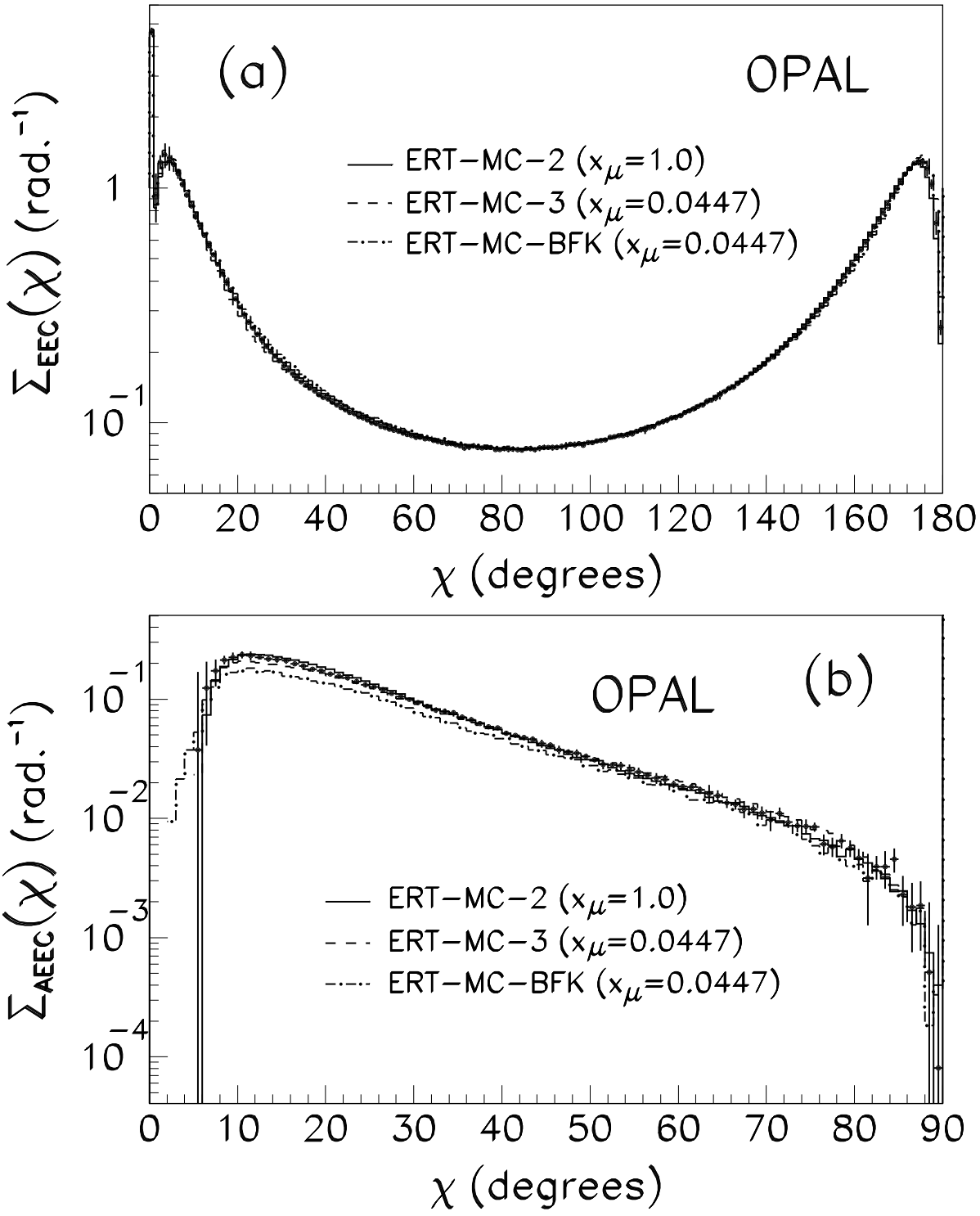
(a)
OPAL
ERT−MC−2 (x_μ=1.0)
ERT−MC−3 (x_μ=0.0447)
ERT−MC−BFK (x_μ=0.0447)
$\Sigma_{EEC}(\chi)$ (rad.$^{-1}$)
1
10^{-1}
0 20 40 60 80 100 120 140 160 180
χ (degrees)
(b)
OPAL
ERT−MC−2 (x_μ=1.0)
ERT−MC−3 (x_μ=0.0447)
ERT−MC−BFK (x_μ=0.0447)
$\Sigma_{AEEC}(\chi)$ (rad.$^{-1}$)
10^{-1}
10^{-2}
10^{-3}
10^{-4}
0 10 20 30 40 50 60 70 80 90
χ (degrees)

Figure 4

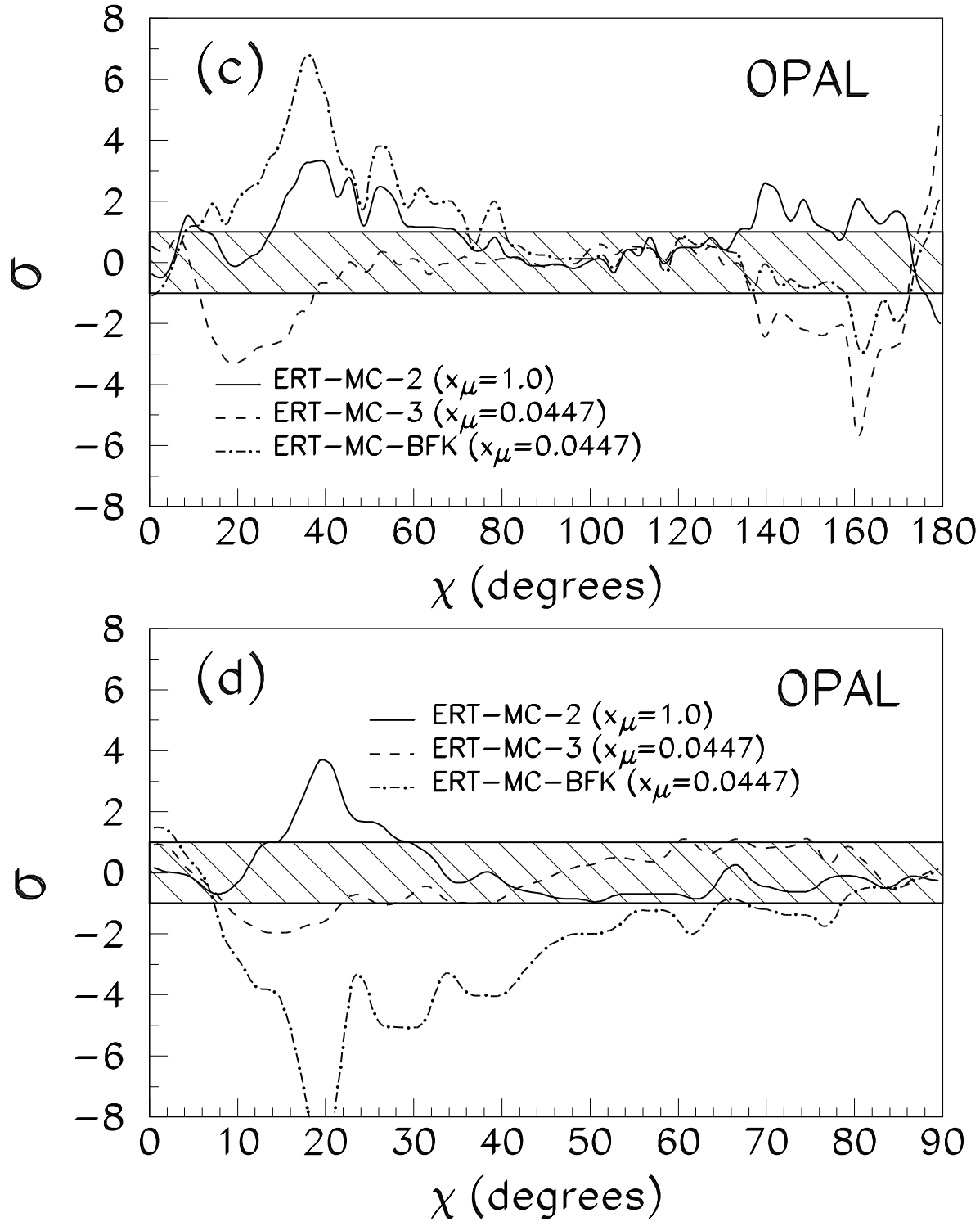
(c)
OPAL
ERT−MC−2 (x_μ=1.0)
ERT−MC−3 (x_μ=0.0447)
ERT−MC−BFK (x_μ=0.0447)
σ
χ (degrees)
(d)
OPAL
ERT−MC−2 (x_μ=1.0)
ERT−MC−3 (x_μ=0.0447)
ERT−MC−BFK (x_μ=0.0447)
σ
χ (degrees)

Figure 5

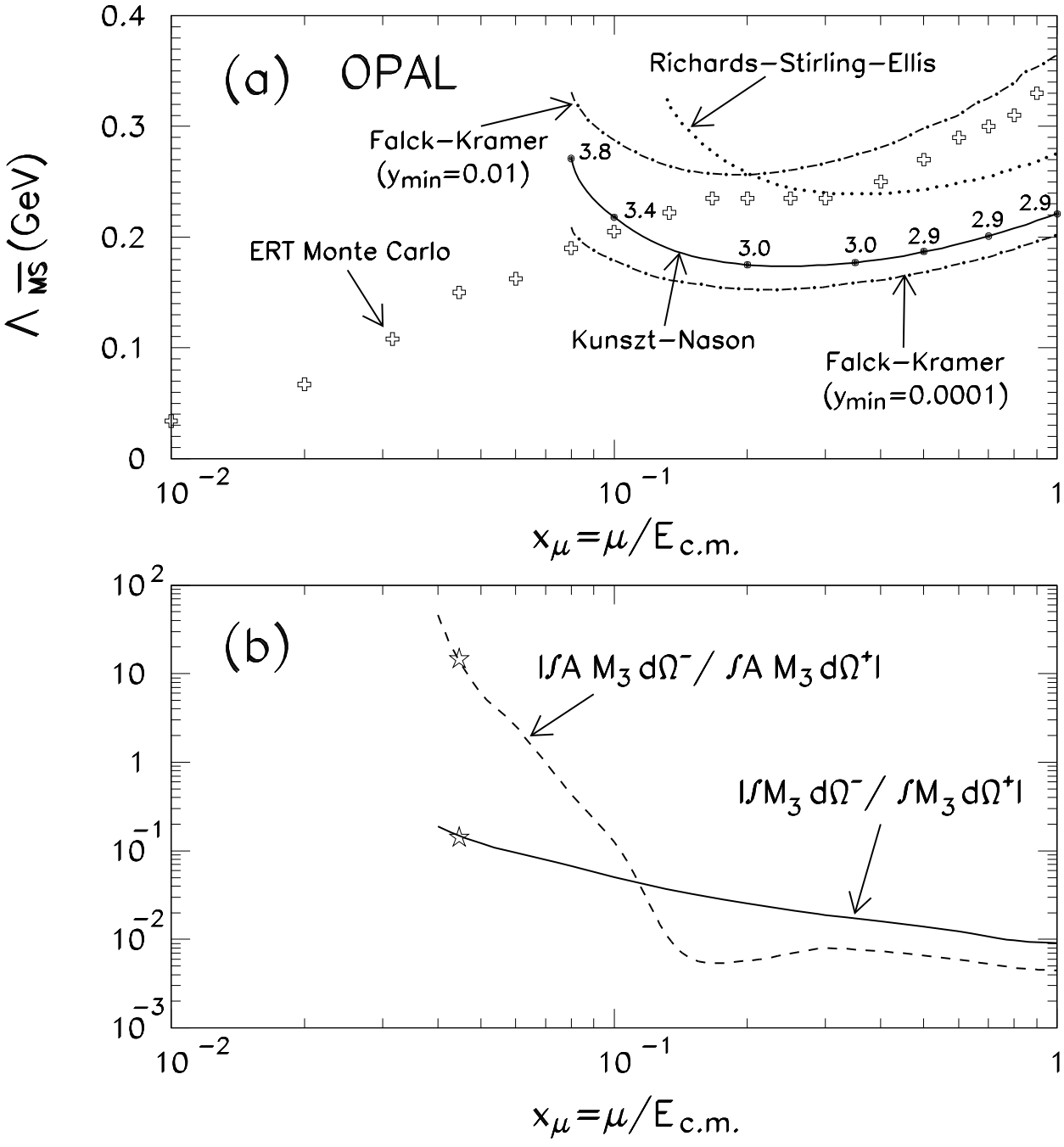
(a) OPAL
Richards–Stirling–Ellis
Falck–Kramer
(y_{min}=0.01)
3.8
3.4
3.0
3.0
2.9
2.9
2.9
ERT Monte Carlo
Kunszt–Nason
Falck–Kramer
(y_{min}=0.0001)
$\Lambda_{\overline{MS}}$ (GeV)
0.4
0.3
0.2
0.1
0
10^{-2}
10^{-1}
1
$x_\mu = \mu / E_{c.m.}$
(b)
$|\int A\, M_3\, d\Omega^- / \int A\, M_3\, d\Omega^+|$
$|\int M_3\, d\Omega^- / \int M_3\, d\Omega^+|$
10^2
10
1
10^{-1}
10^{-2}
10^{-3}
10^{-2}
10^{-1}
1
$x_\mu = \mu / E_{c.m.}$